



## Short communication

## High-performance, ceria-based solid oxide fuel cells fabricated at low temperatures

Zhangbo Liu<sup>a,b,1</sup>, Dong Ding<sup>a,1</sup>, Mingfei Liu<sup>a,1</sup>, Xifeng Ding<sup>a</sup>, Dongchang Chen<sup>a</sup>, Xiaxi Li<sup>a</sup>, Changrong Xia<sup>b</sup>, Meilin Liu<sup>a,c,\*</sup><sup>a</sup> School of Materials Science and Engineering, Center for Innovative Fuel Cell and Battery Technologies, Georgia Institute of Technology, 771 Ferst Drive NW, Atlanta, GA 30332, United States<sup>b</sup> CAS Key Laboratory of Materials for Energy Conversion, Department of Materials Science and Engineering, University of Science and Technology of China, Hefei 230026, Anhui, China<sup>c</sup> Center for New Energy, College of Environment and Energy, South China University of Technology, Guangzhou 510006, China

## HIGHLIGHTS

- Single cells with dense SDC electrolyte are fabricated at low temperatures.
- The cell fabricated at 1150 °C shows higher performance than those made at higher temperatures.
- Adequate long-term stability is demonstrated for the cell fabricated at 1150 °C.
- Electrode polarization at high current densities is significantly suppressed at 650 °C.

## ARTICLE INFO

## Article history:

Received 8 March 2013

Received in revised form

23 April 2013

Accepted 25 April 2013

Available online 3 May 2013

## Keywords:

Ceria

Sintering

Electrolyte

Electrode

Solid oxide fuel cell

## ABSTRACT

To reduce the fabrication cost and avoid unfavorable reactions between components of solid oxide fuel cells, it is necessary to improve the sinterability of the electrolyte materials, especially doped ceria for intermediate-temperature operation. Here we report a unique process for fabrication of single cells at a co-sintering temperature as low as 1150 °C using highly active SDC powders derived from a glycine-nitrate process, demonstrating higher cell performance than those co-sintered at higher temperatures while maintaining adequate long-term stability. In particular, it is found that the electrode polarization at high current densities is significantly suppressed when operated at 650 °C.

© 2013 Elsevier B.V. All rights reserved.

## 1. Introduction

Solid oxide fuel cells (SOFCs) have potential to be the cleanest and the most efficient devices for cost-effective conversion to

electricity of a wide variety of fuels, including hydrogen, hydrocarbons, coal gas, and bio-derived renewable fuels [1–7]. In recent years, intermediate temperature (500–700 °C) SOFCs (IT-SOFCs) have received much attention due to the potential of improved stability and reliability as well as broader materials selection compared with those to be operated at higher temperatures ( $\geq 800$  °C) [8–11]. Doped ceria (DCO), particularly samaria doped ceria (SDC) and gadolinia doped ceria (GDC), are considered as the most promising electrolyte materials for IT-SOFCs, due to their superior ionic conductivity at reduced temperatures, high catalytic activity for both oxygen reduction and fuel reforming, good compatibility with cobalt-based cathodes, as well as similar thermal expansion coefficient to that of Ni-cermet anodes and ferrite stainless steel interconnects [12–18].

Acronyms used: DCO, doped ceria; GDC, gadolinia doped ceria; GNP, glycine-nitrate process; IT-SOFC, intermediate temperature solid oxide fuel cell; OCV, open cell voltage; SDC, samaria doped ceria; SOFC, solid oxide fuel cell; SSC,  $\text{Sm}_{0.5}\text{Sr}_{0.5}\text{CoO}_3$ ; TPB, triple-phase boundary.

\* Corresponding author. School of Materials Science and Engineering, Center for Innovative Fuel Cell and Battery Technologies, Georgia Institute of Technology, 771 Ferst Drive NW, Atlanta, GA 30332, United States. Tel.: +1 404 894 6114; fax: +1 404 894 9140.

E-mail address: [meilin.liu@mse.gatech.edu](mailto:meilin.liu@mse.gatech.edu) (M. Liu).

<sup>1</sup> These authors contribute equally to this work.

However, one of the main drawbacks of DCO-based materials is their poor sinterability, making it difficult to achieve sufficiently high density below 1500 °C [19–21]. The required high firing temperature of the electrolyte would result in a series of problems such as undesired grain growth and interfacial diffusions/reactions between the electrolyte and the electrode during co-firing, which could be detrimental to cell performance and stability. Thus, many efforts have been devoted to improving the sinterability of DCO powders in order to effectively reduce the sintering temperature, to optimize the electrode microstructure, and to minimize or eliminate unfavorable diffusion and reaction between cell components. One approach is to add a small amount of sintering aids such as  $\text{MnO}_2$ ,  $\text{Fe}_2\text{O}_3$ ,  $\text{Co}_3\text{O}_4$ , and  $\text{Li}_2\text{O}$  [22–32]. Another strategy is to develop unique processes for synthesis of ultra-fine DCO powders with higher sinterability, including hydrothermal synthesis, sol–gel, co-precipitation, intensive mechanical milling, and chemical combustion synthesis [15,33–40].

In our recent work, a modified glycine-nitrate process (GNP) using 75 mol%  $\text{Ce}(\text{NO}_3)_3$  and 25 mol%  $\text{Ce}(\text{NH}_4)_2(\text{NO}_3)_6$  as a mixed cerium source was developed to synthesize SDC powders of high sinterability with very low apparent tap density of only  $36.0 \pm 0.5 \text{ mg cm}^{-3}$ . Very dense SDC electrolyte membranes were fabricated from the SDC powders using a co-pressing and co-sintering process; the co-sintering temperature was 1250 °C, and the cells based on the SDC electrolyte showed high OCV and high performance at 600 °C [41]. Due to the high sinterability of the SDC powder derived from the modified GNP, it is expected that the co-sintering temperature of the SDC electrolyte membrane may be further reduced. In this paper, we report our findings on the

microstructure and electrochemical performance of the cells fabricated from the highly-active SDC powders at reduced temperatures: 1200, 1150, and 1100 °C.

## 2. Experimental

### 2.1. Powder synthesis

All powders involved in this work, including SDC, NiO, and  $\text{Sm}_{0.5}\text{Sr}_{0.5}\text{CoO}_3$  (SSC), were synthesized via a GNP as described in detail elsewhere [10,12,41]. Taking the synthesis of SDC powders as an example,  $\text{Sm}(\text{NO}_3)_3 \cdot 6\text{H}_2\text{O}$ ,  $\text{Ce}(\text{NO}_3)_3 \cdot 6\text{H}_2\text{O}$ , and  $\text{Ce}(\text{NH}_4)_2(\text{NO}_3)_6$  (all from Alfa Aesar) were dissolved in distilled water with a molar ratio of 1:3:1, then glycine (Alfa Aesar) was added as both the complexing agent and the fuel with a stoichiometric glycine/nitrate ratio of 28/15 [41]. After sufficiently stirring to achieve complete complexation, the solution was heated on a hotplate till the ignition of a rapid self-sustained combustion, and the resulted ashes were calcined at 600 °C for 2 h to form fluorite phase SDC powders. In the case of NiO and SSC synthesis, the resulted ashes were both calcined at 850 °C for 4 h to get the desired oxides.

### 2.2. Single cell fabrication

Bi-layer pellets consisting of porous NiO–SDC substrate and dense SDC electrolyte were fabricated using a co-pressing and co-sintering process [42,43]. NiO and SDC powders were mixed together to form the precursor of the anode substrate, in which starch (Sigma) was also added as pore former to increase the

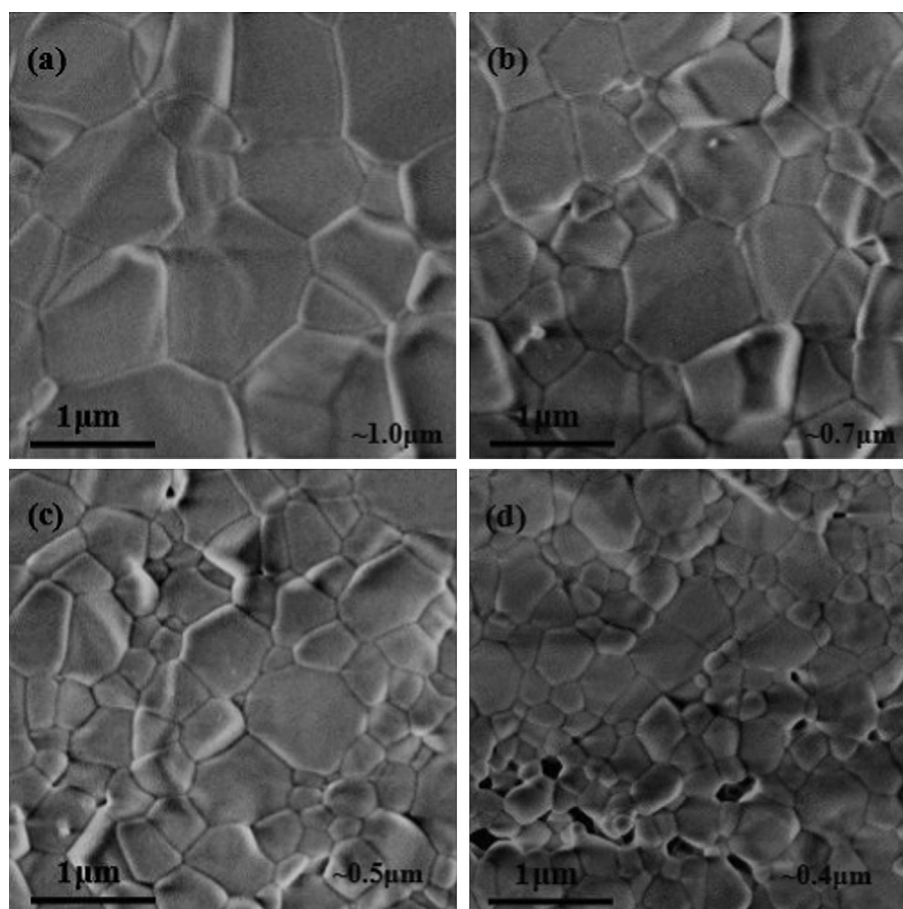
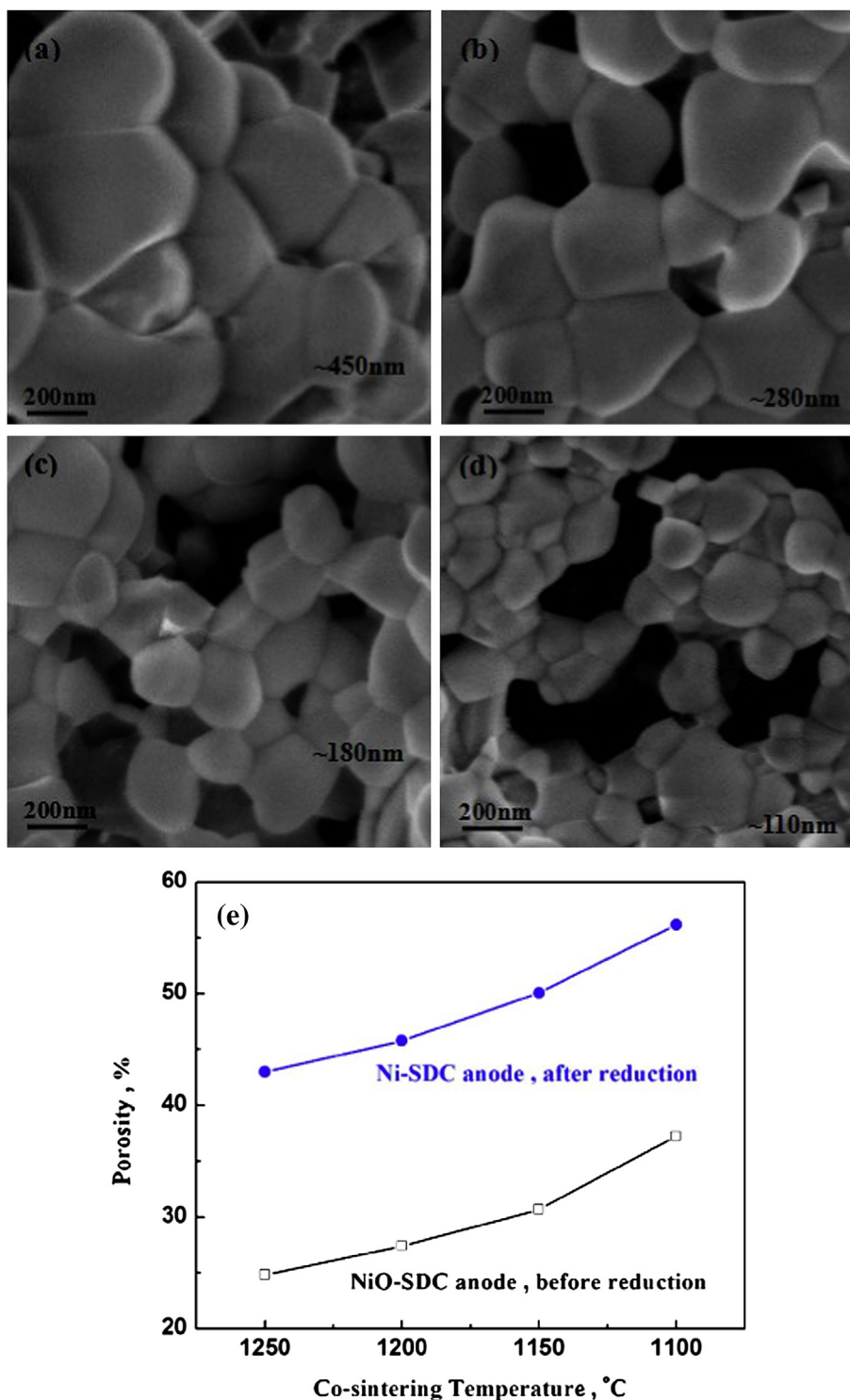


Fig. 1. Cross-sectional views of SDC electrolyte layer of (a) Cell-1250, (b) Cell-1200, (c) Cell-1150 and (d) Cell-1100.

porosity. The mass ratio of NiO, SDC, and starch in the substrate was 65:35:15. The mixed powders were initially compacted at 50 MPa. Then a thin layer of SDC powders was uniformly distributed onto the pre-pressed substrate and uniaxially co-pressed to 250 MPa to form green bi-layer pellets. These bi-layer pellets were subsequently co-sintered at different temperatures, including 1250, 1200, 1150 and 1100 °C for 5 h to densify the electrolyte.

The sintered anode substrate thickness and diameter were  $0.48 \pm 0.01$  mm and  $10.8 \pm 0.2$  mm, respectively, while the thickness of the electrolyte membrane was about  $23.5 \pm 1.0$   $\mu\text{m}$ . Then, SSC and SDC powders with a mass ratio of SSC:SDC = 7:3 were mixed thoroughly with an organic binder (V-006A, Heraeus) to form the cathode slurry, which was subsequently screen-printed onto the electrolyte surface of the sintered bi-layer pellets,



**Fig. 2.** Cross-sectional views of Ni-SDC anodes of (a) Cell-1250, (b) Cell-1200, (c) Cell-1150 and (d) Cell-1100 after reduction at 600 °C for 2 h, (e) porosity of these anodes before and after reduction measured by the Archimedes method.

followed by firing at 950 °C for 2 h. The effective cathode area was 0.3 cm<sup>2</sup>, and the whole process was kept as consistent as possible so that identical cathode polarization resistance could be achieved. For brevity, the cells with anode and electrolyte co-sintered at various temperatures are named as Cell-1250, Cell-1200, Cell-1150 and Cell-1100 thereafter.

### 2.3. Cell testing and characterization

Each single cell was sealed onto an alumina tube using ceramic adhesive (Aremco, Ceramabond 552). NiO paste (Heraeus) and silver paste (Heraeus) were employed as current collector on the anode and the cathode side, respectively, and Ag wire as the lead for both electrodes. Humidified (3% H<sub>2</sub>O) hydrogen was fed to the anode at a flow rate of 30 mL min<sup>-1</sup> as the fuel, while ambient air was used as the oxidant. In addition to measuring the current–voltage curve with an Arbin fuel cell testing system (MSTAT), the electrochemical impedance spectra were measured under open circuit conditions using an EG&G PAR potentiostat (model 273A) interface combined with a Solartron 1255 HF frequency response analyzer. The microstructures of the cells were examined using a scanning electron microscope (SEM, LEO 1530) after polishing and thermal etching at 1100 °C for 10 min, and the porosity of the anode substrate before and after reduction was measured via the Archimedes method.

## 3. Results and discussions

### 3.1. Cell morphologies

Fig. 1 shows some typical cross-sectional views of SDC electrolyte layer of Cell-1250, Cell-1200, Cell-1150, and Cell-1100, suggesting that the SDC electrolyte layer is very dense, even for the sample co-sintered at only 1150 °C. It is noted, however, that some small pin holes are observed on the electrolyte of Cell-1100. Fortunately, these pores are largely isolated from each other so that Cell-1100 was still air-tight for operation. Besides, the average grain size of the SDC electrolyte layer decreased as the co-sintering temperature was reduced.

The morphology of the anode is also dependent sensitively on the co-sintering temperature. Fig. 2 presents some typical cross-sectional views of the Ni–SDC anodes of the test cells after reduction in humidified hydrogen at 600 °C for 2 h. As expected, the grain size decreased significantly as the co-sintering temperature was reduced. The porosity of the anodes before and after reduction was measured using the Archimedes method, as plotted in Fig. 2e. When the co-sintering temperature was reduced from 1250 to 1100 °C, the porosity of the NiO–SDC substrate increased by ~12.4%, from 24.8 ± 0.4% to 37.2 ± 0.4%. After reduction at 600 °C for 2 h, the porosity of each anodes further increased by ~19%, reaching 56.2 ± 0.4% for Cell-1100. Higher porosity and finer grain size are very favorable for rapid fuel/product transport and electrochemical reactions, thus higher performance. Reducing the co-firing temperature would help to increase porosity while reducing grain size of the electrodes.

### 3.2. Cell performance at 600 °C

Fig. 3a shows some typical current–voltage curves of the cells co-sintered at different temperatures, as tested at 600 °C with humidified hydrogen (3% H<sub>2</sub>O) as fuel and ambient air as oxidant. As can be seen clearly, Cell-1250 exhibits an OCV of ~0.901 V, a rather high value for SOFCs based on thin-film DCO electrolyte at this operation temperature [10,44]. Moreover, a peak power density of ~0.762 W cm<sup>-2</sup> is achieved for this cell. The OCV

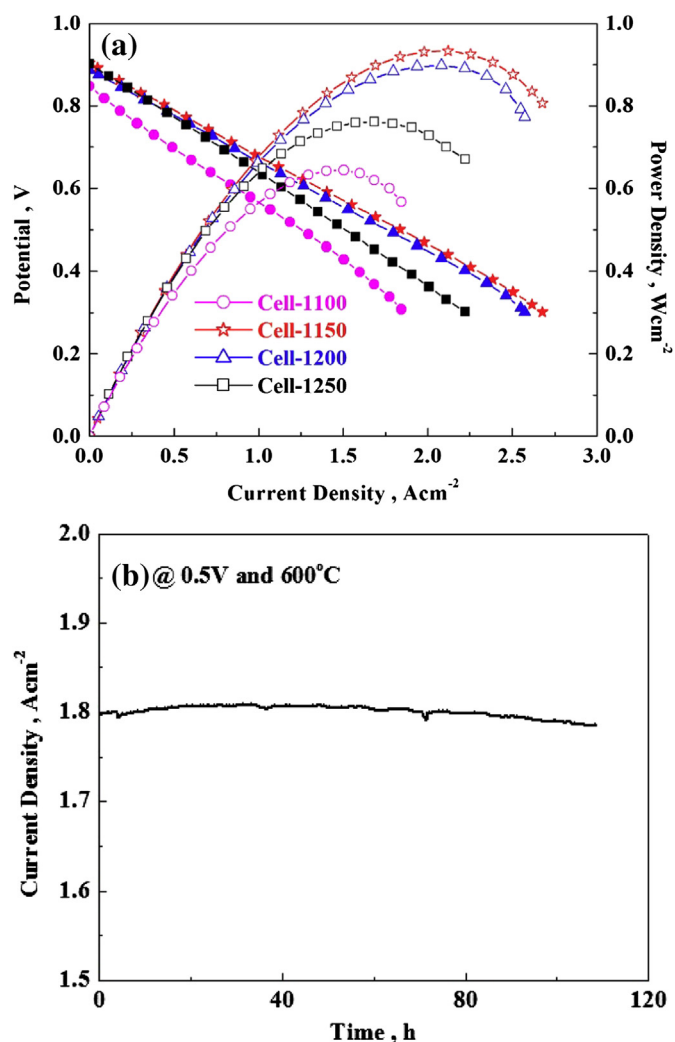


Fig. 3. (a) Dependence of cell voltage and power density on current density for various cells, and (b) current density as a function of time at a constant voltage of 0.5 V for Cell-1150 at 600 °C, when humidified H<sub>2</sub> (3% H<sub>2</sub>O) and ambient air are used as the fuel and the oxidant, respectively.

values remained relatively constant as the co-sintering temperature was reduced to 1200 and 1150 °C, indicating that the SDC film was dense at these lower sintering temperatures. Besides, the output performance increased significantly as the co-sintering temperature was reduced. Cell-1200 demonstrated a peak power density of ~0.898 W cm<sup>-2</sup>, which increased to ~0.933 W cm<sup>-2</sup> for Cell-1150. It is believed that the increased performance is attributed to finer microstructure of the anode and hence larger number of active sites for electrochemical reactions [45,46]. Further lowering the co-sintering temperature to 1100 °C, however, leads to a sharp decrease in both OCV and cell performance, due probably to the relatively lower density of the SDC electrolyte layer. Consequently, 1150 °C is an optimized co-sintering temperature for thin-film SDC based cells fabricated by this co-pressing technique. Moreover, Cell-1150 displayed good stability, as shown in Fig. 3b.

To obtain more detailed information, typical electrochemical impedance spectra are acquired under open circuit conditions with a two-electrode configuration, as shown in Fig. 4a. The ohmic resistances are obtained from the high frequency intercepts with the real axis, and the total polarization resistances  $R_p$  are determined from the following equation [47]:

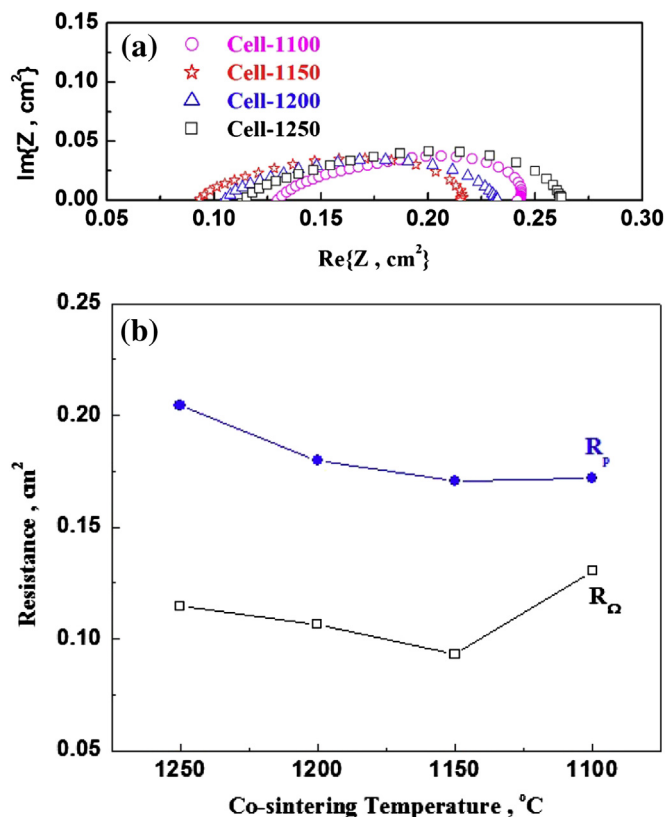


Fig. 4. (a) Impedance spectra measured under open circuit conditions, and (b) calculated  $R_{\Omega}$  and  $R_p$ , for various cells at 600 °C.

$$R_p = \frac{R_t - R_{\Omega}}{\frac{V_{oc}}{E_n} \left[ 1 - \frac{R_{\Omega}}{R_t} \left( 1 - \frac{V_{oc}}{E_n} \right) \right]} \quad (1)$$

where  $E_n$  is the Nernst potential at 600 °C,  $V_{oc}$  is the measured OCV,  $R_{\Omega}$  is the ohmic resistance, and  $R_t$  is the total resistance determined from the low frequency intercept with the real axis in the impedance spectra.  $R_{\Omega}$  and the calculated  $R_p$  are then plotted versus the co-sintering temperature in Fig. 4b. It is seen that both  $R_p$  and  $R_{\Omega}$  were decreased as the co-sintering temperature was reduced from 1250 to 1200 and 1150 °C ( $R_p$  was decreased from 0.204 to 0.180 and 0.171  $\Omega \text{ cm}^2$ , respectively, while  $R_{\Omega}$  was decreased from 0.114 to 0.107 and 0.093  $\Omega \text{ cm}^2$ , respectively), due most likely to extended effective triple phase boundary (TPB) and improved anode–electrolyte interface with optimized anode microstructures [45,46]. However, when the co-sintering temperature was further reduced to 1100 °C,  $R_{\Omega}$  increased significantly due to lower density of the electrolyte membrane as shown in Fig. 1d.

### 3.3. Cell performance at different temperatures

The cells were also tested at 550 and 650 °C, as shown in Fig. 5a. It is clear that Cell-1150 showed the best performance at the all operating temperatures studied: 550, 600 and 650 °C. Even at 550 °C, a peak power density as high as 0.620  $\text{W cm}^{-2}$  was achieved for that cell.

Shown in Fig. 5b are some typical current–voltage curves of the cells tested at 650 °C. As expected, the OCVs of the cells were significantly lower than the values obtained at 600 °C (see Fig. 3a), due to increased electronic transference number of DCO electrolyte at higher temperatures. The OCVs of Cell-1200 and Cell-1150 are

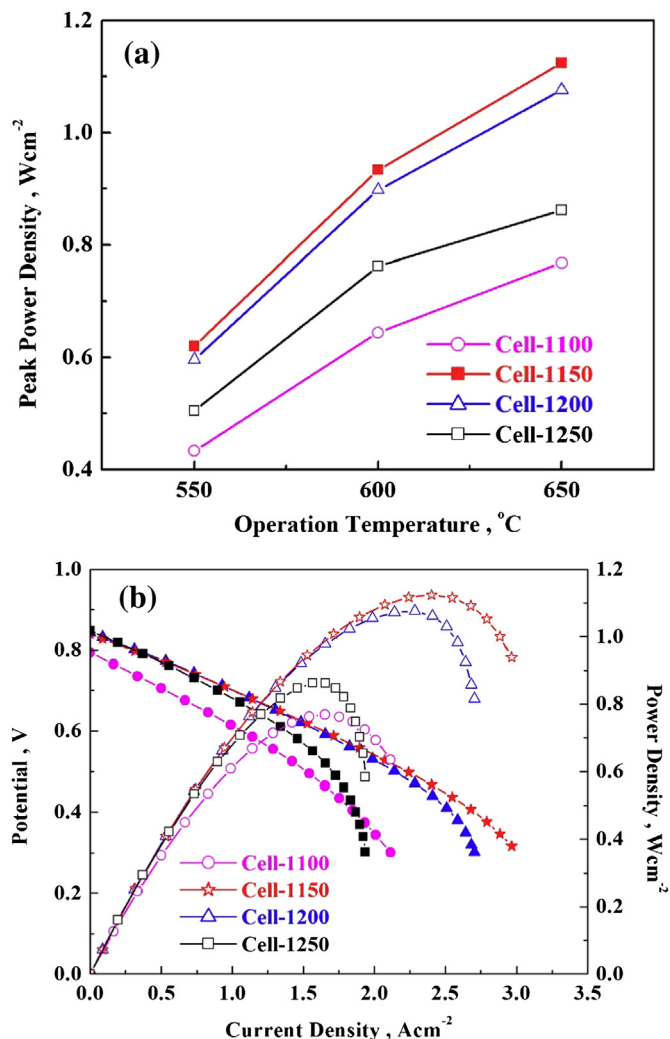


Fig. 5. (a) Peak power density measured at different temperatures, and (b) dependence of cell voltage and power density on current density at 650 °C for various cells, when humidified  $\text{H}_2$  (3%  $\text{H}_2\text{O}$ ) and ambient air are used as the fuel and the oxidant, respectively.

still very close to that of Cell-1250 ( $\sim 0.845 \text{ V}$ ), but Cell-1100 displayed a much lower OCV ( $\sim 0.795 \text{ V}$ ), due to insufficient density of the DCO electrolyte membrane.

On the other hand, it is noted that Cell-1150 and Cell-1200 showed significantly higher cell performance than Cell-1250 under typical operating conditions. For example, a peak power density as high as  $\sim 1.124 \text{ W cm}^{-2}$  was demonstrated by Cell-1150 and  $\sim 1.076 \text{ W cm}^{-2}$  by Cell-1200. In contrast, Cell-1250 showed a peak power density of only  $\sim 0.862 \text{ W cm}^{-2}$ . It appears that the increased porosity of the anodes co-fired at lower temperatures may facilitate the rate of the electrochemical processes and enhanced the cell performance. In addition, it is found that the electrode polarization at high current densities is significantly suppressed when the co-sintering temperature is reduced.

## 4. Conclusion

In summary, we have successfully fabricated high-performance, single cells by co-pressing followed by co-sintering at a temperature as low as 1150 °C using highly-active SDC powders derived from a modified glycine-nitrate process, which uses 75 mol%  $\text{Ce}(\text{NO}_3)_3$  and 25 mol%  $\text{Ce}(\text{NH}_4)_2(\text{NO}_3)_6$  as a mixed cerium source. In particular, the

low firing temperature has resulted in anode microstructures with more appropriate porosity, grain size, and connectivity with the electrolyte, significantly reducing both the ohmic resistance and the electrode polarization and enhancing cell performance.

## Acknowledgment

This material is based upon work supported as part of the Heterogeneous Functional Materials (HetroFoaM) Center, an Energy Frontier Research Center funded by the U.S. Department of Energy, Office of Science, Office of Basic Energy Sciences under Award Number DE-SC0001061. Zhangbo Liu acknowledges a fellowship from the China Scholarship Council.

## References

- [1] B.C.H. Steele, A. Heinzel, *Nature* 414 (6861) (2001) 345–352.
- [2] Z.L. Zhan, S.A. Barnett, *Science* (2005) 844–847.
- [3] Y.H. Huang, et al., *Science* (2006) 254–257.
- [4] L. Yang, et al., *Science* (2009) 126–129.
- [5] Z. Cheng, et al., *Energy & Environmental Science* 4 (11) (2011) 4380–4409.
- [6] M. Liu, et al., *Materials Today* 14 (11) (2011) 534–546.
- [7] M. Liu, et al., *Nano Energy* 1 (3) (2012) 448–455.
- [8] D.J.L. Brett, et al., *Chemical Society Reviews* 37 (8) (2008) 1568–1578.
- [9] Z. Jiang, et al., *Electrochimica Acta* 55 (11) (2010) 3595–3605.
- [10] Z. Liu, et al., *Journal of Power Sources* 196 (20) (2011) 8561–8567.
- [11] Z. Shao, et al., *Progress in Materials Science* 57 (4) (2012) 804–874.
- [12] C. Xia, et al., *Solid State Ionics* 149 (1–2) (2002) 11–19.
- [13] C. Fu, et al., *Electrochimica Acta* 52 (13) (2007) 4589–4594.
- [14] D. Pérez-Coll, et al., *Journal of Power Sources* 173 (1) (2007) 291–297.
- [15] D. Ding, et al., *Solid State Ionics* 179 (21–26) (2008) 896–899.
- [16] C. Ding, et al., *Journal of Dispersion Science and Technology* 30 (2) (2009) 241–245.
- [17] D. Ding, et al., *Electrochimica Acta* 55 (15) (2010) 4529–4535.
- [18] C. Gaudillere, et al., *Catalysis Today* 157 (1–4) (2010) 263–269.
- [19] T. Kudo, H. Obayashi, *Journal of the Electrochemical Society* 122 (1) (1975) 142–147.
- [20] R. Gerhardt-Anderson, A.S. Nowick, *Solid State Ionics* 5 (0) (1981) 547–550.
- [21] H. Yahiro, et al., *Journal of the Electrochemical Society* 135 (8) (1988) 2077–2080.
- [22] C. Kleinogel, L.J. Gauckler, *Solid State Ionics* 135 (1–4) (2000) 567–573.
- [23] C. Kleinogel, L.J. Gauckler, *Advanced Materials* 13 (14) (2001) 1081–1085.
- [24] T.S. Zhang, et al., *Solid State Ionics* 168 (1–2) (2004) 187–195.
- [25] H. Yoshida, T. Inagaki, *Journal of Alloys and Compounds* 408–412 (2006) 632–636.
- [26] T.S. Zhang, et al., *Journal of Alloys and Compounds* 422 (1–2) (2006) 46–52.
- [27] X. Zhang, et al., *Journal of Power Sources* 162 (1) (2006) 480–485.
- [28] J.D. Nicholas, L.C. De Jonghe, *Solid State Ionics* 178 (19–20) (2007) 1187–1194.
- [29] C.J. Fu, et al., *International Journal of Hydrogen Energy* 35 (20) (2010) 11200–11207.
- [30] M. Han, et al., *Journal of Materials Science & Technology* 27 (5) (2011) 460–464.
- [31] Y. Zheng, et al., *International Journal of Hydrogen Energy* 36 (8) (2011) 5128–5135.
- [32] S. Li, et al., *Journal of Power Sources* 205 (2012) 57–62.
- [33] J. VanHerle, et al., *Solid State Ionics* 86–8 (1996) 1255–1258.
- [34] R.S. Torrens, et al., *Solid State Ionics* 111 (1–2) (1998) 9–15.
- [35] S. Dikmen, et al., *Solid State Sciences* 4 (5) (2002) 585–590.
- [36] E. Ruiz-Trejo, et al., *Journal of Solid State Chemistry* 180 (11) (2007) 3093–3100.
- [37] R.O. Fuentes, R.T. Baker, *International Journal of Hydrogen Energy* 33 (13) (2008) 3480–3484.
- [38] D.H. Prasad, et al., *Journal of the European Ceramic Society* 28 (16) (2008) 3107–3112.
- [39] A. Moure, et al., *Journal of the European Ceramic Society* 29 (12) (2009) 2559–2565.
- [40] W.S. Jung, et al., *Ceramics International* 36 (1) (2010) 371–374.
- [41] Z. Liu, et al., *Journal of Power Sources* 229 (1) (2013) 277–284.
- [42] C. Xia, M. Liu, *Journal of the American Ceramic Society* 84 (8) (2001) 1903–1905.
- [43] C. Xia, M. Liu, *Solid State Ionics* 144 (3–4) (2001) 249–255.
- [44] X. Zhang, et al., *Journal of Power Sources* 160 (2) (2006) 1211–1216.
- [45] T. Suzuki, et al., *Science* 325 (5942) (2009) 852–855.
- [46] S. Gamble, *Materials Science and Technology* 27 (10) (2011) 1485–1497.
- [47] M. Liu, H. Hu, *Journal of the Electrochemical Society* (1996) L109–L112.